Pentagonal monolayer crystals of carbon, boron nitride, and silver azide

M. Yagmurcukardes,[1,a)] H. Sahin,[2] J. Kang,[2] E. Torun,[2] F. M. Peeters,[2] and R. T. Senger[1,b)]
[1]*Department of Physics, Izmir Institute of Technology, 35430 Urla, Izmir, Turkey*
[2]*Department of Physics, University of Antwerp, Campus Groenenborgerlaan, 2020, Antwerp, Belgium*

(Received 4 June 2015; accepted 24 August 2015; published online 8 September 2015)

In this study, we present a theoretical investigation of structural, electronic, and mechanical properties of pentagonal monolayers of carbon (p-graphene), boron nitride (p-B_2N_4 and p-B_4N_2), and silver azide (p-AgN_3) by performing state-of-the-art first principles calculations. Our total energy calculations suggest feasible formation of monolayer crystal structures composed entirely of pentagons. In addition, electronic band dispersion calculations indicate that while p-graphene and p-AgN_3 are semiconductors with indirect bandgaps, p-BN structures display metallic behavior. We also investigate the mechanical properties (in-plane stiffness and the Poisson's ratio) of four different pentagonal structures under uniaxial strain. p-graphene is found to have the highest stiffness value and the corresponding Poisson's ratio is found to be negative. Similarly, p-B_2N_4 and p-B_4N_2 have negative Poisson's ratio values. On the other hand, the p-AgN_3 has a large and positive Poisson's ratio. In dynamical stability tests based on calculated phonon spectra of these pentagonal monolayers, we find that only p-graphene and p-B_2N_4 are stable, but p-AgN_3 and p-B_4N_2 are vulnerable against vibrational excitations. © *2015 AIP Publishing LLC*.
[http://dx.doi.org/10.1063/1.4930086]

I. INTRODUCTION

In the last decade, graphene, one atom thick form of carbon atoms arranged in a honeycomb structure, has become one of the most exciting topics of materials research due to its exceptional properties.[1,2] Besides graphene,[3] there exists many other forms of pure carbon in nature such as graphite, diamond, C_{60} fullerene,[4] nanotube,[5] carbon nanocone,[6] nanochain,[7] and graphdiyne,[8] which are the well known bulk and low dimensional forms of carbon element. In addition to these, stability and unique mechanical properties of a new carbon allotrope, p-graphene, are reported by Zhang *et al.* recently.[9] It is shown that while the unique pentagonal crystal symmetry provides a dynamical stability (for temperatures up to 1000 K), the buckled nature of the p-graphene leads to a negative value for its Poisson's ratio.

The synthesis of graphene[3,10] made other two dimensional materials, such as hexagonal structures of III–V binary compounds,[11,12] a popular field of research. Moreover, one-dimensional forms of AlN and BN, as nanotubes and nanoribbons were studied before.[13–18] Hexagonal monolayer structures of these compounds, for example, *h*-BN[19,20] and *h*-AlN[11,21–25] are wide band-gap semiconductors with a non-magnetic ground state. Recently, the synthesis of *h*-AlN by Tsipas *et al.*[26] motivated further study of the properties of *h*-AlN. Very recently, we have reported unique thickness-dependent features of the electronic structure of *h*-AlN crystal.[21]

Metal azides, consisting of a metal atom (Na, K, Rb, Cs, Ag, Cu, or Tl) and the azide molecule (N_3), are another group of compounds which may find applications in monolayer crystal technology. Their electronic structure, chemical bonding, vibrational, and optical properties have been investigated.[27–40] Due to its large chemical energy stored in its bulk phases, AgN_3 is one of the intensely studied members of this family. Gordienko *et al.*[27] have studied the electronic band structure of AgN_3 by using density functional theory (DFT) calculations. Jain *et al.*[28] calculated the energy band gap of AgN_3 as 2.95 eV. In addition, in the study by Aluker *et al.*,[29] the chemical bonding between the Ag and N atoms were studied by using a pseudopotential approach. Using a pseudoatomic orbital basis, the electronic structure of AgN_3 was also reported.[30] Change of structural and vibrational properties of AgN_3 under applied pressure was studied by using DFT and generalized gradient approximation (GGA).[31] Moreover, Schmidt *et al.*[32] reported the crystal structure and chemical bonding of the high temperature phase of AgN_3 by using X-ray powder diffraction. In this study, it was pointed out that the high temperature-AgN_3 phase contains buckled layers with silver atom connecting to the azide groups in pentagonal form in the direction parallel to [001]. The phase transitions and structures of AgN_3 at different pressure values were also reported by Hou *et al.*[33]

In this study, we investigate the structural, electronic, and mechanical properties of pentagonal monolayers of carbon (p-graphene), two phases of boron nitride (p-B_2N_4 and p-B_4N_2), and silver azide (p-AgN_3). The mechanical properties of these pentagonal structures are examined under uniaxial strain and in terms of the in-plane stiffness and the Poisson's ratio values. Their vibrational spectra are also calculated. The paper is organized as follows: The details of our computational methodology are given in Sec. II. Structural properties of four different pentagonal structures are presented in Sec. III. The electronic and magnetic properties of optimized structures are investigated in Sec. IV. In Sec. V, mechanical properties and dynamical stability of the

a)Electronic mail: mehmetyagmurcukardes@iyte.edu.tr
b)Electronic mail: tugrulsenger@iyte.edu.tr

TABLE I. Geometry of pentagonal structures, calculated lattice parameter a, the distance between atoms d_{XY}, buckling of the monolayer h, total magnetic moment μ, the amount of charge lost or gained by the atoms $\Delta\rho$, the total cohesive energy of a primitive unit cell E_c, the energy band gap of the structure E_g, work function Φ, Poisson's ratio ν, and in-plane stiffness C.

	Geometry	a (Å)	d_{XY} (Å)	h (Å)	M (μ_B)	$\Delta\rho$ (e)	E_c (eV)	E_g (eV)	Φ (eV)	ν	C (eV/Å^2)
p-graphene	Buckled	3.64	1.34 (C_1-C_1) 1.55 (C_1-C_2)	1.21	0	0.3	42.40	2.21	6.01	−0.08	16.71
p-AgN_3	Planar	6.01	1.19 (N-N) 2.33 (Ag-N)	…	0	2.1	31.45	1.33	3.43	0.90	0.37
p-B_2N_4	Buckled	3.62	1.34 (N-N) 1.55 (B-N)	1.26	0	4.2	34.49	…	5.19	−0.02	3.62
p-B_4N_2	Buckled	3.79	1.59 (B-B) 1.57 (N-B)	1.23	1.95	4.3	33.58	…	3.88	−0.19	7.59

pentagonal structures are investigated. Finally, we present our conclusions in Sec. VI.

II. COMPUTATIONAL METHODOLOGY

In this study, the first-principles calculations were performed within the framework of DFT by using the Vienna *Ab initio* Simulation Package (VASP) package.[41–44] The approach is based on an iterative solution of the Kohn-Sham equations[45] with a plane-wave set adopted with the Perdew-Burke-Ernzerhof (PBE) exchange-correlation functional of the GGA.[46,47] In order to analyze the charge transfers the Bader technique was used.[48]

Electronic and geometric relaxations of the pentagonal structures of the monolayers were performed by considering the following criteria in our calculations. The energy cut-off value for plane wave basis set was taken to be 500 eV. The global break condition for the electronic self consistent-loop was considered to be 10^{-5} eV. For geometric relaxation of the structures, primitive unit cells containing 6 or 8 atoms were considered. For this purpose, the minimum energy was calculated by varying the lattice constant values, and the pressure in all directions is decreased to a value smaller than 1 kbar. Brillouin zone integration was performed by using a set of $5 \times 5 \times 1$ Gamma-centered k-point sampling mesh. For density of states and work function calculations, a set of $15 \times 15 \times 1$ k-point sampling was used to get more accurate results. The cohesive energy of a unit cell was calculated using the formula $E_c = \sum n_a E_a - E_{str}$, where E_a denotes the energy of a single isolated atom and n_a denotes the number of atoms contained in the unit cell. E_{str} denotes the total energy of the monolayer structure. Summation is used for the structure containing different types of atoms in its simulation cell. Calculated cohesive energies are listed in Table I.

III. STRUCTURAL PROPERTIES

First, geometrical relaxations of structures were performed by considering their square-shaped primitive unit cells with the lattice vectors $a_1 = a(1,0,0)$ and $a_2 = a(0,1,0)$ for all structures (see Fig. 1). In the structure of p-graphene the 4-coordinated carbon atoms were denoted by C_1 while the 3-coordinated ones were denoted by C_2. The geometrical calculations show that the bond length of C_1-C_2 is 1.55 Å while C_2-C_2 bond length is 1.34 Å. The lattice constant is $a = 3.64$ Å within GGA, and it is consistent with the value calculated by Zhang *et al.*[9] The buckling of the layer is 1.21 Å, which is also consistent with the value calculated by Zhang *et al.*[9] Bader charge analysis indicates that 0.3 e amount of charge is donated from C_1 and two C_2 atoms to other two C_2 atoms. The calculated cohesive energy is 42.40 eV for p-graphene monolayer.

For p-AgN_3 geometry relaxation, 8-atomic primitive unit cell was considered. As seen in Fig. 1(b), 2-coordinated N atoms are denoted by N_1 while 3-coordinated ones are denoted by N_2. The geometry relaxation within the GGA gives the lattice constant value as $a = 6.02$ Å. The Ag-N_1 bond length is 2.33 Å while the N_1-N_2 bond length is 1.19 Å. The bond angle between the Ag-N_1-Ag atoms is 132.5° and it is 90° for the N_1-Ag-N_1 bonds. The relaxed geometry of AgN_3 monolayer structure is planar similar to some other two dimensional structures such as hexagonal graphene and h-BN. Bader charge analysis shows that an amount of 0.7 e charge from each Ag atom is donated to the N atoms but dominantly to the central ones. The final charge on the Ag, N_1 and N_2 atoms and N_1 atom are 10.3 e, 5.2 e, and 5.3 e,

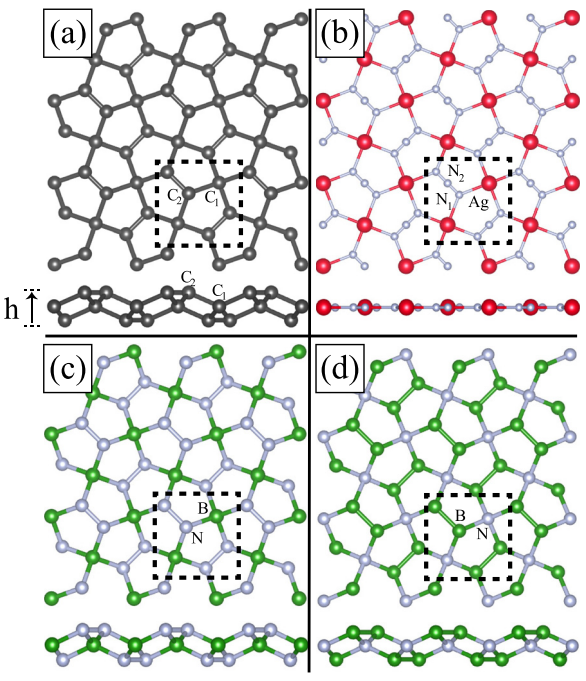

FIG. 1. Top view and side view of pentagonal (a) graphene (b) AgN_3, (c) B_2N_4, and (d) B_4N_2.

respectively. The total cohesive energy of p-AgN_3 is 31.45 eV, as listed in Table I.

Optimized lattice constant of the p-B_2N_4 is found to be $a = 3.62$ Å. The N-N and B-N bond lengths are 1.34 Å and 1.55 Å, respectively. The buckling of p-B_2N_4 is 1.26 Å, which is close to that of p-graphene. The Bader charge analysis demonstrates that B atoms have final charge of 0.9 e so that an amount of 2.1 e charge is transferred to the N atoms from each B atom. The cohesive energy of p-B_2N_4 monolayer is calculated as 34.49 eV.

The p-B_4N_2 has a lattice constant of $a = 3.79$ Å, which is greater than that of p-B_2N_4. This time the B-N bond length is 1.57 Å while the B-B bond length is 1.59 Å. The buckling of p-B_4N_2 is 1.23 Å, which is close to that of the p-B_2N_4 structure. Results of Bader charge analysis indicates that an amount of 2.2 e charge is depleted to each N atom from the B atoms. Finally, the cohesive energy of p-B_4N_2 is 33.58 eV.

IV. ELECTRONIC PROPERTIES

In this section, the electronic band dispersion and magnetic ground state of p-graphene, p-AgN_3, p-B_2N_4, and p-B_4N_2 are investigated comprehensively. As seen in Table I, the p-graphene has an indirect band gap of 2.21 eV. As shown in Fig. 2(a), the valence band maximum (VBM) of the p-graphene is located in between the Γ and the X (high symmetry) points while the conduction band minima (CBM) is in between the M and the Γ points. It also appears that the both spin up and spin down states are degenerate throughout the Brillouin Zone, and thus, the structure does not exhibit any spin polarization in its ground state. In the 6-atomic primitive unit cell of the p-graphene while two of the 4-coordinated C atoms have no excess electrons, four 3-coordinated C atoms pair their electrons in p_z orbitals, and therefore, the p-graphene has a nonmagnetic ground state.

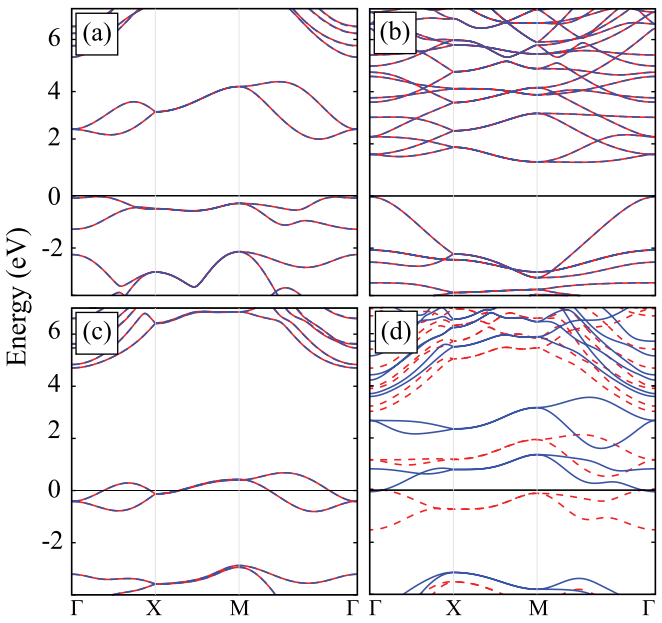

FIG. 2. Band-structures of pentagonal (a) graphene (b) AgN_3, (c) B_2N_4, and (d) B_4N_2, where blue lines denote up spins while dashed red lines denote down spins, respectively.

The p-AgN_3 has an indirect band gap of 1.33 eV as seen in Table I. In Fig. 2(b), the VBM of the p-AgN_3 is in between the Γ and the X points while the CBM exists in between the M and the Γ points. As shown in Fig. 2(b) the p-AgN_3 also does not exhibit any spin.

The p-B_2N_4 is another structure having nonmagnetic ground state. As shown in Fig. 2(c), again the spin up and the spin down states are degenerate. Unlike the p-graphene and the p-AgN_3, the p-B_2N_4 displays metallic behavior. The valence band crosses the Fermi level in between all high symmetry points through whole Brillouin Zone.

In all the pentagonal structures considered, only the p-B_4N_2 has a spin polarization in its ground state. The total magnetic moment of p-B_4N_2 is 1.95 μ_B as given in Table I. This value of total magnetic moment arises from the ferromagnetic ordering of B local moments. In the primitive unit cell, each B atom has a local magnetic moment of 0.48 μ_B, while the each N atom has local moment about 0.02 μ_B, which is very small compared to that of B atom. Therefore, the net magnetic moment of 1.95 μ_B for p-B_4N_2 structure is mostly due to local moments of B atoms. In its 6-atomic primitive unit cell both N atoms are 4-coordinated while all the B atoms are 3 coordinated. The spin polarization is localized on the N atoms since they add up their electrons in their p_z orbitals. As given in Fig. 2(d), the spin up and spin down states have different dispersions. Only in between the high symmetry points Γ and the X, M, and the Γ, the spin up and spin down bands cross each other just above the Fermi level. The valence band of spin down states crosses Fermi level while the conduction band of spin up states crosses Fermi level. The band structure metallic for both spins but if spin orbit coupling is included, then there may open a band gap at the points where the up and down spin bands cross.

The charge density difference plots of pentagonal structures are provided in Fig. 3. In order to plot these figures, we first obtained the total charge density of each material. Then, using the same unit cell and settings we obtained the charge

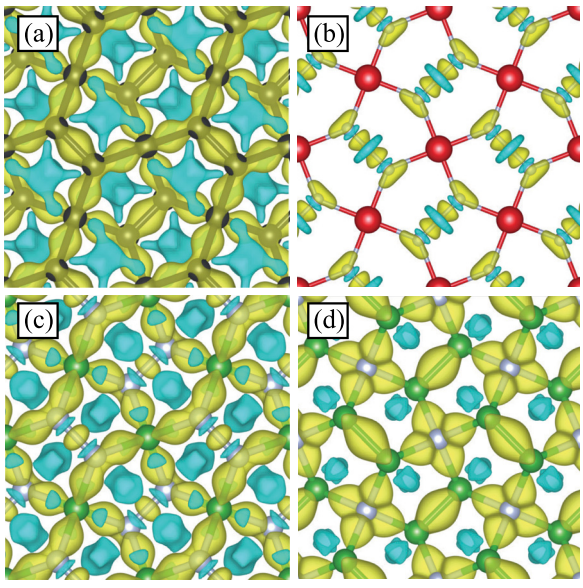

FIG. 3. Charge density difference of pentagonal (a) graphene, (b) AgN_3, (c) B_2N_4, and (d) B_4N_2.

density of each atom separately at their original positions in the compound. After that, we summed these individual charge densities and subtracted them from the charge density of the compound. These figures reveal the modifications in the total charge of the individual atoms when the crystal is formed. The charge density difference plot of p-graphene in Fig. 3(a) shows that there is a charge depletion in the hollow site of the lattice. This charge is accumulated mostly at the bonding sited between the C atoms. Fig. 3(b) indicates that, for the AgN_3, there is a charge depletion from the N_2 atoms and a charge accumulation at the region where the N_1-N_2 and N_1-Ag chemical bonds are formed. The hollow site charge depletion is also observed for B_2N_4 in Fig. 3(c). Similar to previous cases, there is a charge accumulation at the locations where the B-N chemical bonds are formed. For the case of B_4N_2 in Fig. 3(d), there is a charge depletion from the one side of the B atoms and again a charge accumulation at the bonding sites.

For the p-graphene, the charge transfer is from C_1 atoms and 2 of C_2 atoms to other C_2 atoms. For the p-AgN_3, as shown in Fig. 3(b), there exists a charge depletion from Ag and N_1 atoms to central N atoms in azide group. For the p-B_2N_4 structure, all of the charge given in Table I is depleted to the N atoms as depicted by the charge density plot in Fig. 3(c). Finally, for p-B_4N_2 monolayer, again the charge depletion occurs from B atoms to N atoms.

V. MECHANICAL PROPERTIES

The stiffness can be explained as the rigidity or the flexibility of a material. The parameter which shows the mechanical response of a material to an applied stress is called the Poisson's ratio. It is defined as the ratio of the transverse contraction strain to the longitudinal extension strain in the direction of stretching force. The in-plane stiffness and the Poisson's ratio can be deduced from the relationship between the strain and the total energy. To calculate the mentioned parameters, we apply strain ε_x and ε_y to these materials by changing the lattice constants along x and y directions. The strain range is from -0.02 to 0.02 with a step of 0.01, which gives a data grid of 25 points. At each grid point, the atomic positions are relaxed, and the strain energy E_S, which is the energy difference between strained and unstrained structures, is calculated. In the harmonic region the strain energy can be fitted as $E_S = c_1\varepsilon_x^2 + c_2\varepsilon_y^2 + c_3\varepsilon_x\varepsilon_y$. The in-plane stiffness along x and y directions can then be calculated as $C_x = (1/S_0)(2c_1 - c_3^2/2c_2)$ and $C_y = (1/S_0)(2c_2 - c_3^2/2c_1)$, where S_0 is the unstretched area of the supercell. The Poisson's ratio along x and y directions can be obtained by $\nu_x = c_3/2c_2$ and $\nu_y = c_3/2c_1$, respectively. For all pentagonal structures, we find that the in-plane stiffness and the Poisson's ratio along x and y directions are equal.

The calculated in-plane stiffness and Poisson's ratio are listed in Table I. It can be seen that p-graphene has the largest in-plane stiffness of 16.71 eV/Å^2, indicating strong bonding between carbon atoms. However, this value is smaller than that of graphene, which has an in-plane stiffness of 20.91 eV/Å^2.[16] This can be attributed to different number of bonds in p-graphene and graphene. In graphene, each C atom is 3-fold coordinated, while in graphyne, the average coordination number of C atom is 2.67. P-graphene has fewer number of bonds than graphene, so it has relatively smaller in-plane stiffness. The calculated Poisson's ratio for p-graphene is -0.08, which is consistent with the value calculated by Zhang *et al.*[9]

The p-AgN_3 has a large Poisson's ratio of 0.90, revealing its strong ability to preserve the equilibrium area when strain is applied. The Poisson's ratio for p-B_4N_2 is -0.19, which is consistent with the calculation of in-plane stiffness. P-B_2N_4 has an in-plane stiffness of 3.62 eV/Å^2, much smaller than the p-graphene. For p-B_4N_2, the in-plane stiffness is 7.59 eV/Å^2. It is interesting to note that the p-graphene, the p-B_2N_4, and the p-B_4N_2 have negative Poisson's ratio values, contrary to the most of the existing materials. Therefore, they belong to the so-called auxetic structures. When uniaxial tensile strain is applied to these structures, the lattice along the transverse direction expands rather than compresses. Normally, this ratio is positive and most of the solids expand in the transverse direction when they are subjected to a uniaxial compression. The materials with negative Poisson's ratio unfold when they are stretched. Therefore, they are isotropic in two dimensions for certain lengths and angles. It has been reported that some artificial materials have negative Poisson's ratio and they exhibit excellent mechanical properties.[49,50] In contrast to structure-engineered bulk auxetics, the negative Poisson's ratio is intrinsic in single layers of p-graphene, p-B_2N_4, and p-B_4N_2.

We also consider higher values of strain from 0.04 to 0.40 in uniform expansion, in order to see structural deformations and determine the elastic and plastic regions for each pentagonal structure. For this purpose, we prefer a fully symmetric square lattice with well defined high symmetry points in the BZ. Again, the calculations are performed in a 2×2 supercell. Increasing the strength of applied strain, increases the total energy of the structure. The p-graphene has no structural deformation up to the strain value of 40%, but the buckling of the layer decreases to 0.66 Å. Under 40% strain, the C_2-C_2 and C_1-C_2 bond lengths are 1.35 Å and 2.15 Å, respectively. P-AgN_3 also does not have any structural deformation up to 40% strain. It remains in the same form but with a higher Ag-N_1 bond length of 3.47 Å, while the bond lengths in azide group remain the same. The situation is different for pentagonal structures of B and N, because they both have deformations in their structures at some critical strain values. P-B_2N_4 has no pentagonal shape structure when 12% strain is applied. Therefore, one may say that it is the critical strain value for p-B_2N_4 between elastic and plastic regions. Plastic region refers to a region in which irreversible structural changes occur in the system and it transforms into a different structure. This critical strain value is slightly greater for p-B_4N_2. After the strain strength of 16%, p-B_4N_2 transforms into a different structure (Fig. 4).

As an important feature of mechanical properties, we also examine the dynamical stability of pentagonal monolayer structures by performing phonon calculations. Here, the dynamical matrix and the vibrational modes were

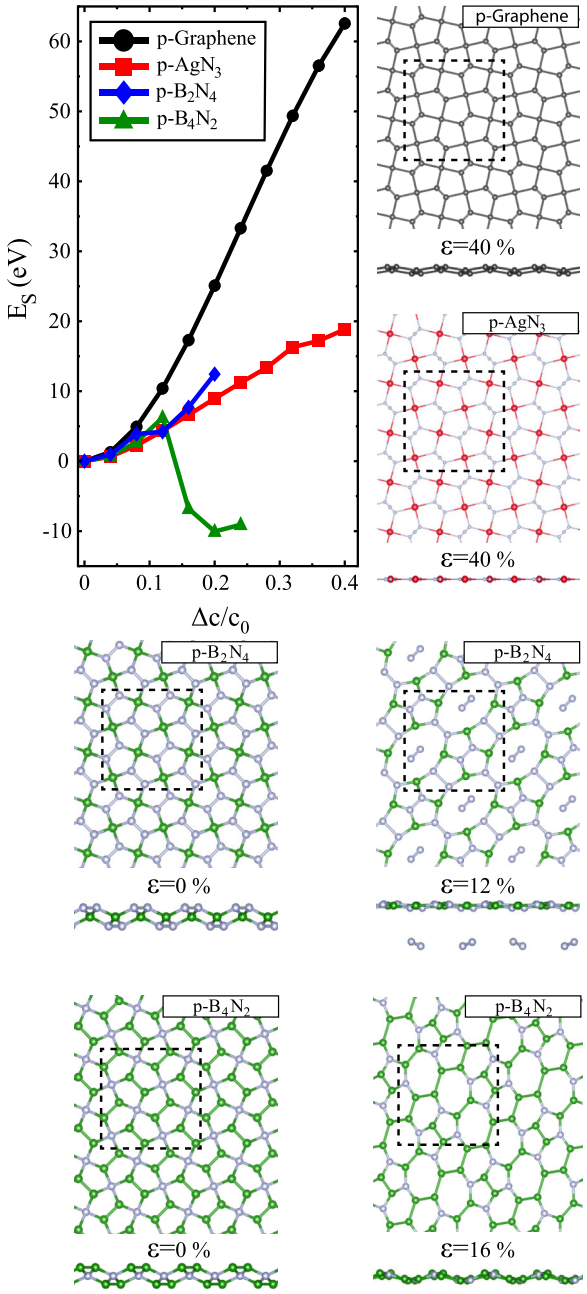

FIG. 4. Energy variation of the pentagonal structures under applied strain and the corresponding atomic configurations at given strain strengths.

calculated using the small-displacement method (SDM)[51] with forces obtained from VASP. As shown in Fig. 5, while pentagonal structures of graphene and B_2N_4 have real vibrational eigenfrequencies in the whole Brillouin zone, p-AgN_3 and p-B_4N_2 have some phonon branches with zero-frequency modes at several points in the Brillouin zone. This is an indication of irreversible deformations that can be induced by those vibrational modes. It appears that although the total energy calculations yield optimized atomic structures of p-AgN_3 and p-B_4N_2 these structures are dynamically unstable. Our calculations also reveal that p-graphene and p-B_2N_4 not only possess dynamically stable crystal structures but also have quite high-frequency phonon modes indicating strong bond formation in these materials.

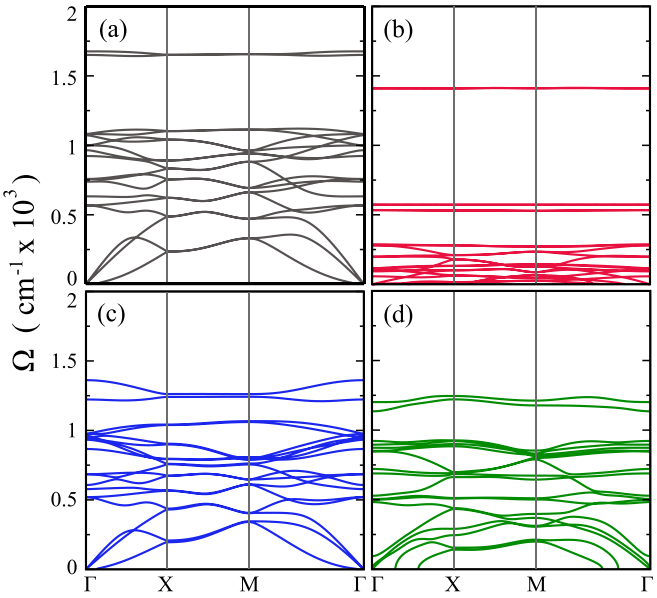

FIG. 5. Phonon modes of pentagonal (a) graphene (b) AgN_3, (c) B_2N_4, and (d) B_4N_2.

VI. CONCLUSIONS

Motivated by the unique properties of the recently reported p-graphene, we have investigated the structural, mechanical, and electronic properties of three novel pentagonal structures as well as p-graphene. Our calculations demonstrate that pentagonal structures of graphene and BN have buckled geometries, while p-AgN_3 has a planar geometry. Calculated band structures show that although hexagonal graphene is a zero-band gap semiconductor, the band dispersion of p-graphene displays an indirect-band-gap semiconductor behavior. Also, the band dispersion of p-AgN_3 displays semiconducting behavior with an indirect band gap. However, pentagonal structures of BN are metallic while hexagonal BN monolayer is a wide-band-gap semiconductor. For all of the pentagonal structures investigated in this study, only p-B_4N_2 has a magnetic ground state while the other structures have nonmagnetic ground states. We have also studied the mechanical properties of these structures and calculated their in-plane stiffness and corresponding Poisson's ratios. The stiffest monolayer is found to be the p-graphene among the four structures. p-graphene, p-B_2N_4, and p-B_4N_2 all have negative Poisson's ratio while the p-AgN_3 has a positive Poisson's ratio. Also, the uniform strain calculations indicate that p-graphene and p-AgN_3 do not show any irreversible structural deformations for up to large strain values while p-B_2N_4 and p-B_4N_2 deform into different phases at some certain strain strengths.

ACKNOWLEDGMENTS

This work was supported by the Flemish Science Foundation (FWO-Vl) and the Methusalem foundation of the Flemish government. Computational resources were provided by TUBITAK ULAKBIM, High Performance and Grid Computing Center (TR-Grid e-Infrastructure). H.S. was supported by a FWO Pegasus Long Marie Curie Fellowship.

H.S. and R.T.S. acknowledge the support from TUBITAK through Project No. 114F397.

[1]K. S. Novoselov, A. K. Geim, S. V. Morozov, D. Jiang, Y. Zhang, S. V. Dubonos, I. V. Grigorieva, and A. A. Firsov, Science **306**, 666 (2004).
[2]K. S. Novoselov, A. K. Geim, S. V. Morozov, D. Jiang, M. I. Katsnelson, I. V. Grigorieva, S. V. Dubonos, and A. A. Firsov, Nature **438**, 197 (2005).
[3]A. K. Geim and K. S. Novoselov, Nat. Mater. **6**, 183 (2007).
[4]H. W. Kroto, J. R. Heath, S. C. O'Brien, R. F. Curl, and R. E. Smalley, Nature **318**, 162 (1985).
[5]S. Iijima and T. Ichihashi, Nature **363**, 603 (1993).
[6]J. C. Charlier and G. M. Rignanese, Phys. Rev. Lett. **86**, 5970 (2001).
[7]C. Jin, H. Lan, L. Peng, K. Suenaga, and S. Iijima, Phys. Rev. Lett. **102**, 205501 (2009).
[8]Y. Li, L. Xu, H. Liu, and Y. Li, Chem. Soc. Rev. **43**, 2572 (2014).
[9]S. Zhang, J. Zhou, Q. Wang, X. Chen, Y. Kawazoe, and P. Jena, Proc. Natl. Acad. Sci. U.S.A. **112**, 2372 (2015).
[10]C. Berger, Z. Song, X. Li, X. Wu, N. Brown, C. Naud, D. Mayou, T. Li, J. Hass, A. N. Marchenkov, E. H. Conrad, P. N. First, and W. A. de Heer, Science **312**, 1191 (2006).
[11]K. S. Novoselov, D. Jiang, F. Schedin, T. Booth, V. V. Khot-kevich, S. Morozov, and A. K. Geim, Proc. Natl. Acad. Sci. U.S.A. **102**, 10451 (2005).
[12]H. Sahin, S. Changirov, M. Topsakal, E. Bekaroglu, E. Akturk, R. T. Senger, and S. Ciraci, Phys. Rev. B **80**, 155453 (2009).
[13]Z. Zhang and W. Guo, Phys. Rev. B **77**, 075403 (2008).
[14]C. H. Park and S. G. Louie, Nano Lett. **8**, 2200 (2008).
[15]V. Barone and J. E. Peralta, Nano Lett. **8**, 2210 (2008).
[16]M. Topsakal, E. Akturk, and S. Ciraci, Phys. Rev. B **79**, 115442 (2009).
[17]M. W. Zhao, Y. Y. Xia, D. J. Zhang, and L. M. Mei, Phys. Rev. B **68**, 235415 (2003).
[18]C. Y. F. Zhukovskii, A. I. Popov, C. Balasubramanian, and S. Bellucci, J. Phys. Condens. Matter **18**, S2045 (2006).
[19]H. Zeng, C. Zhi, Z. Zhang, X. Wei, X. Wang, W. Guo, Y. Bando, and D. Golberg, Nano Lett. **10**, 5049 (2010).
[20]L. Song, L. Ci, H. Lu, P. B. Sorokin, C. Jin, J. Ni, A. G. Kvashnin, D. G. Kvashnin, J. Lou, B. I. Yakobson, and P. M. Ajayan, Nano Lett. **10**, 3209 (2010).
[21]C. Bacaksiz, H. Sahin, H. D. Ozaydin, S. Horzum, R. T. Senger, and F. M. Peeters, Phys. Rev. B **91**, 085430 (2015).
[22]H. L. Zhuang and R. G. Hennig, Appl. Phys. Lett. **101**, 153109 (2012).
[23]Q. Wang, Q. Sun, P. Jena, and Y. Kawazoe, ACS Nano **3**, 621 (2009).
[24]K. K. Kim, A. Hsu, X. Jia, S. M. Kim, Y. Shi, M. Hofmann, D. Nezich, J. F. Rodriguez-Nieva, M. Dresselhaus, T. Palacios, and J. Kong, Nano Lett. **12**, 161 (2012).
[25]M. Farahani, T. S. Ahmadi, and A. Seif, J. Mol. Struct. **913**, 126 (2009).
[26]P. Tsipas, S. Kassavetis, D. Tsoutsou, E. Xenogiannopoulou, E. Golias, S. A. Giamini, C. Grazianetti, D. Chiappe, A. Molle, M. Fanciulli, and A. Dimoulas, Appl. Phys. Lett. **103**, 251605 (2013).
[27]A. B. Gordienko, Y. N. Zhuravlev, and A. S. Poplavnoi, Phys. Status Solidi B **198**, 707 (1996).
[28]P. Jain, J. Sahariya, H. S. Mund, M. Sharma, and B. L. Ahuja, Comput. Mater, Sci. **72**, 101 (2013).
[29]E. D. Aluker, Y. N. Zhuravlev, V. Y. Zakharov, N. G. Kravchenko, V. I. Krasheninin, and A. S. Poplavnoi, Russ. Phys. J. **46**, 855 (2003).
[30]A. B. Gordienko and A. S. Poplavnoi, Russ. Phys. J. **47**, 1056 (2004).
[31]W. Zhu and H. Xiao, J. Solid State Chem. **180**, 3521 (2007).
[32]C. L. Schmidt, R. Dinnebier, U. Wedig, and M. Jansen, Inorg. Chem. **46**, 907 (2007).
[33]D. Hou, F. Zhang, C. Ji, T. Hannon, H. Zhu, J. Wu, V. I. Levitas, and Y. Ma, J. App. Phys. **110**, 023524 (2011).
[34]A. B. Gordienko and A. S. Poplavnoi, J. Struct. Chem. **46**, 968 (2005).
[35]W. Zhu and H. Xiao, J. Compd. Chem. **29**, 176 (2008).
[36]W. Zhu and H. Xiao, Struct. Chem. **21**, 657 (2010).
[37]B. L. Evans, A. D. Yoffe, and P. Gray, Chem. Rev. **59**, 515 (1959).
[38]B. L. Evans and A. D. Yoffe, Proc. R. Soc. London, Ser. A **250**, 346 (1959).
[39]R. J. Colton and J. W. Rabalaist, J. Chem. Phys. **64**, 3481 (1976).
[40]B. P. Aduev, E. D. Aluker, G. M. Belokurov, Y. A. Zakharov, and A. G. Krechetov, J. Exp. Theor. Phys. **89**, 906 (1999).
[41]G. Kresse and J. Hafner, Phys. Rev. B **47**, 558 (1993).
[42]G. Kresse and J. Hafner, Phys. Rev. B **49**, 14251 (1994).
[43]G. Kresse and J. Furthmüller, Comput. Mater. Sci. **6**, 15 (1996).
[44]G. Kresse and J. Furthmüller, Phys. Rev. B **54**, 11169 (1996).
[45]W. Kohn and L. J. Sham, Phys. Rev. **140**, A1133 (1965).
[46]J. P. Perdew, K. Burke, and M. Ernzerhof, Phys. Rev. Lett. **77**, 3865 (1996).
[47]J. P. Perdew, K. Burke, and M. Ernzerhof, Phys. Rev. Lett. **78**, 1396 (1997).
[48]G. Henkelman, A. Arnaldsson, and H. Jonsson, Comput. Mater. Sci. **36**, 354 (2006).
[49]S. Burns, Science **238**, 551 (1987).
[50]J. W. Jiang and H. S. Park, Nat. Commun. **5**, 4727 (2014).
[51]D. Alfe, Comput. Phys. Commun. **180**, 2622 (2009).